Published in final edited form as:
Biochemistry. 2009 October 20; 48(41): 9891–9902. doi:10.1021/bi9008853.

Structural Insights of Glucan Phosphatase Dynamics using Amide Hydrogen/Deuterium Exchange Mass Spectrometry

Simon Hsu[1], **Youngjun Kim**[2], **Sheng Li**[1], **Eric S. Durrant**[1], **Rachel M. Pace**[3], **Virgil L. Woods Jr.**[1], and **Matthew S. Gentry**[3]

[1]Department of Medicine, University of California-San Diego, La Jolla, CA 92093-0601

[2]Department of Applied Biochemistry, Konkuk University, 322 Danwol-dong, Chungju-city, Chungbuk, 380-701, Korea

[3]Department of Molecular and Cellular Biochemistry, University of Kentucky, Lexington, KY 40536

Abstract

Laforin and Starch Excess 4 (SEX4) are founding members of a class of phosphatases that dephosphorylate phosphoglucans. Each protein contains a carbohydrate binding module (CBM) and a dual specificity phosphatase (DSP) domain. The gene encoding laforin is mutated in a fatal neurodegenerative disease called Lafora disease (LD). In the absence of laforin function, insoluble glucans accumulate that are hyperphosphorylated and exhibit sparse branching. It is hypothesized that these accumulations trigger the neurodegeneration and premature death of LD patients. We recently demonstrated that laforin removes phosphate from phosphoglucans and hypothesized that this function inhibits insoluble glucan accumulation. Loss of SEX4 function in plants yields a similar cellular phenotype; cells accumulate an excess amount of insoluble, hyperphosphorylated glucans. While multiple groups have shown that these phosphatases dephosphorylate phosphoglucans, there is no structure of a glucan phosphatase and little is known about the mechanism whereby they perform this action. We utilized hydrogen-deuterium exchange mass spectrometry (DXMS) and structural modeling to probe the conformational and structural dynamics of the glucan phosphatase SEX4. We found that the enzyme does not undergo a global conformational change upon glucan binding, but instead undergoes minimal rearrangement upon binding. The CBM undergoes increased protection from deuteration when bound to glucans, confirming its role in glucan binding. More interestingly, we identified structural components of the DSP that also undergo increased protection from deuteration upon glucan addition. To determine the position of these regions, we generated a homology model of the SEX4 DSP. The homology model shows that all of these regions are adjacent the DSP active site. Therefore, our results suggest that these regions of the DSP participate in presenting the phosphoglucan to the active site and provide the first structural analysis and mode of action of this unique class of phosphatases.

Corresponding authors: Matthew Gentry, Ph.D., 741 S. Limestone, BBSRB, B177, Lexington, KY 40536-0509; Tel.: 859.323.8482; Fax: 859.323.5505; matthew.gentry@uky.edu, or Virgil Woods, Jr., M.D. Tel.: 858.534.2180; Fax: 858.534.2606; vwoods@ucsd.edu.

SUPPORTING INFORMATION

The supporting information includes: a FPLC trace showing the gel-filtration purification of monomeric Δ81-SEX4-C198S (Figure S1), peptides within the dual specificity phosphatase (DSP) domain that exhibit less than 10% change in deuterium incorporation between Apo and amylopectin-bound prior to the 30,000 s time point (Figure S2), peptides outside of the DSP and CBM that exhibit less than 10% change in deuterium incorporation (Figure S3), deuterium exchange results of Apo and amylopectin-bound Δ81-SEX4 (Figure S4), and predicted secondary structure and domain topography of full-length SEX4 (Figure S5). This material is available free of charge via the Internet at http://pubs.acs.org.

Keywords

phosphatase; neurodegenerative disease; Lafora disease; glycogen; starch; SEX4; laforin; carbohydrate binding module

The major storage carbohydrate/glucan in plants and animals is starch and glycogen, respectively. Both polymers are composed of α-1,4-glycosidic linkages between glucose residues with branches attached by α-1,6-glycosidic linkages. The major differences between the two polymers is that glycogen exhibits consistent branching every 12-14 glucose monomers and amylopectin, the major component of starch, exhibits clustered branching every 12-20 glucose monomers and clustered regions with no branching. These differences in branching patterns largely accounts for the fact that glycogen is water soluble and starch is insoluble.

Lafora disease (LD; OMIM #254780) is an autosomal recessive neurodegenerative disease that results in epilepsy and death around age thirty (1,2). A hallmark of LD is the accumulation of insoluble glucans called Lafora bodies (LBs) (3,4). Glycogen, the normal energy storage glucan in metazoans, is water soluble, regularly branched, and sparsely phosphorylated. Alternatively, LBs are sparsely branched, hyperphosphorylated glucans that are water insoluble and closely resemble amylopectin, the major component of plant starch (5-7). Mutations in the gene encoding laforin result in LD (8,9). Laforin is a bimodular protein composed of a carbohydrate binding module (CBM) followed by a dual specificity phosphatase (DSP) domain (8-10). We recently demonstrated that laforin has the unique activity of dephosphorylating phosphoglucans (11,12). Additionally, laforin is the only phosphatase in vertebrate genomes with a CBM, and as such the only phosphatase predicted to possess this activity. Recent work from our lab, and others, has suggested that laforin dephosphorylates nascent glucans during glycogen metabolism to inhibit LB formation, but the mechanism of this action and the details of this proposed pathway are still being elucidated (11-17).

The *Starch Excess 4* (*SEX4*) gene is conserved in all members of Archaeplastida/Kingdom Plantae (18). Mutations in *SEX4* result in excess starch accumulation in *Arabidopsis* cells (19,20). This cellular phenotype is similar to the cellular phenotype observed in LD patients, i.e. excess insoluble glucan accumulation. The SEX4 protein is composed of a chloroplast Targeting Peptide (cTP), followed by a DSP domain, and then a CBM (19,21). Similar to laforin, SEX4 also binds and dephosphorylates phosphoglucans, and we recently demonstrated that laforin can functionally replace SEX4 (11).

In plants, unlike in vertebrates, significant progress has been made in understanding phosphoglucan metabolism as a means to store and access energy caches (22-25). The emerging theme for starch breakdown in *Arabidopsis* is as follows: glucose monomers on the surface of starch are phosphorylated on the C6- and C3-position by glucan water dikinase (GWD) and phosphoglucan water dikinase (PWD), respectively; β-amylase cleaves glucose polymers and releases maltose; the glucan phosphatase SEX4 releases phosphates; and the debranching enzyme isoamylase hydrolyzes branch points while α-amylase releases oligosaccharides (22-26). In the absence of SEX4 activity, β-amylase activity is inhibited and α-amylase releases phospho-oligosaccharides (22). Thus, there is a coordinated phosphorylation and dephosphorylation of the glucan that is necessary for proper starch breakdown.

Little is known regarding the structural dynamics of glucan phosphatases, i.e. how the two domains interact both prior and during glucan binding. In addition, the structural properties that allow glucan phosphatases to accommodate a phosphoglucan in their active site, rather than the typical phospho-peptide, are entirely unknown. Therefore, we set out to determine if conformational changes occur upon glucan binding and to identify the regions of SEX4 that

interact with phosphoglucans, being particularly interested in if/how the phosphatase domain of SEX4 interacts with phosphoglucans. Deuterium exchange techniques have been employed to probe protein structure for more than 50 years (27,28). In more recent years, deuterium exchange has been coupled with pepsin proteolysis, HPLC separation, and mass spectrometry and further developed into a powerful technique known as deuterium exchange-mass spectrometry (DXMS) (29-31).

Since there is no available structure of a glucan phosphatase and only limited structural information about glucan phosphatases, we probed the conformational and dynamic changes of the glucan phosphatase SEX4 upon glucan binding using DXMS. Upon glucan binding, we observed a decrease in deuteration of multiple peptides, but did not observe any substantial increases in deuteration. These results indicate that SEX4 does not undergo a large-scale conformational change when it binds glucans. We observed decreases in deuteration in both the CBM and DSP domain. We found that upon glucan binding the proposed regions of the CBM that bind the glucan are more resistant to deuteration. This result is as expected, since the glucan would inhibit deuteration to this region upon binding. More surprisingly, we found that bound glucan also protected specific regions of the DSP domain from deuteration. A homology model of the SEX4 DSP revealed that each of these regions is adjacent the SEX4 DSP active site and suggests that these regions participate in phosphoglucan presentation to the SEX4 active site. Thus, we present the first data that elucidates a mechanistic action of a glucan phosphatase.

EXPERIMENTAL PROCEDURES

Protein Expression, purification, and Western analysis

Δ81-SEX4, Δ52-SEX4, and all mutants were expressed with a C-terminal His_6-tag in *Escherichia coli* BL21 (DE3) CodonPlus cells (Stratagene). Most of the fusion proteins were expressed and purified from soluble bacterial extracts using Ni^{2+}-agarose affinity chromatography as previously described (32). The Δ81-SEX4-C198S used in DXMS studies was purified using a Profinia IMAC column (Bio-Rad) with a Profinia protein purification system (Bio-Rad). Monomeric Δ81-SEX4–C198S from the Profinia was purified to near homogeneity using a HiLoad 16/60 Superdex 200 size exclusion column (GE Healthcare) and concentrated to 10 mg/ml. Purifications were performed in 20 mM Tris-HCl, 100 mM NaCl, 15 mM imidazole, and 2 mM dithiothreitol (DTT) at pH 7.2. Western analysis was performed on HIS-tagged proteins using mouse α-6xHIS (NeuroMab) and goat α-mouse-HRP (Zymed).

Optimization of pepsin digestion of SEX4

Target protein digestion by pepsin is a requisite step prior to DXMS experiments. In optimizing this process, the total number of peptides produced from pepsin digestion was evaluated under several different conditions including concentrations of denaturant. For each sample test, 5 μl of Δ81-SEX4-C198S was diluted in 15 μl of 100 mM NaCl, 2 mM DTT, 7.8 mM Tris pH 7.1 (on ice), representing the dilution of the protein into D_2O based buffers in deuterium-exchange experiments. The sample was then diluted with 30 μl of a cold quench solution (0° C) of 0.8% formic acid, 16.6% glycerol, and guanidine hydrochloride (GuHCl) at final concentrations of 0.05 M, 0.5 M, 1.0 M, 2.0 M, or 4.0 M. This quenching step represented the reduction of hydrogen-deuterium exchange with a decrease in pH to 2.2 -2.5 in addition to denaturing the protein prior to pepsin proteolysis with GuHCl and acidic conditions. The quenching/denaturation process was allowed to proceed on ice for 30 seconds, after which, the sample was frozen by submersion into dry ice. The frozen sample was stored at −80 °C until transferred to the dry ice-containing sample basin of the cryogenic autosampler module of the DXMS apparatus. Procedures for pepsin digestion for DXMS have been described (33-36). Briefly, the sample was thawed at 0 °C, injected and pumped through a porcine pepsin

immobilized column (Sigma), and the protease generated peptides were collected on a C18 HPLC column (Vydac). The column effluent was analyzed on an LCQ Classic (Thermo Finnigan Inc.) electrospray ion trap-type mass spectrometer and an electrospray Q-TOF mass spectrometer (Micromass). Determination of pepsin-generated peptide sequences from the resulting MS:MS data sets was facilitated through the use of SEQUEST (Finnigan, Inc.).

Hydrogen/deuterium exchange

DXMS experiments were performed as previously described (33-37). Δ81-SEX4-C198S samples were prepared with three states of hydrogen-deuterium exchange in each deuterium exchange experiment, consisting of nondeuterated (ND), deuterated, and fully deuterated (FD). The nondeuterated sample was processed exactly as described in the digestion optimization described in the previous paragraph. The FD sample represents the “maximum” hydrogen–deuterium exchange for a certain time period, which in these experiments was a period of 24 h where the samples were allowed to exchange at room temperature in D_2O buffer (1% (v/v) formic acid). The deuterated samples represent different incubation times prior to the quenching of the exchange process. Briefly, a 5 μl solution of Δ81-SEX4-C198S (10 mg/mg) was diluted with 15 μl of ice cold D_2O buffer (7.8 mM Tris-HCl, 100 mM NaCl, at pH 7.1 ± 5 mM β-cyclodextrin), samples were incubated at 0°C for 10 s, 30 s, 100 s, 300 s, 1000 s, 3000 s, and 10,000 s (166.67 min), then mixed with 30 μl of quench solution (0.8% (v/v) formic acid, 0.08 M guanidine hydrochloride, 16.6% (v/v) glycerol) with samples on ice for 30 seconds, and then samples were transferred to ice-cooled autosampler vials, frozen on dry ice, and stored at −80°C. In amylopectin binding experiments, Δ81-SEX4-C198S was pre-incubated with 5 mg/ml amylopectin (Sigma) at room temperature for 30 minutes and then chilled to 0 °C. The pepsin digestion (16 s), chromatography, and the mass spectral acquisition proceeded as described in the digestion optimization section. This process is an automated system, such that the time between protein loading onto pepsin and mass spectral acquisition is constant (~7 min) for each sample. All of the samples for one protein were prepared and run on the same day. Each Apo and amylopectin-bound DXMS experiment was performed a minimum of three times and for each experiment we prepared and analyzed samples in triplicate. The ribbon maps and graphs are the average percent deuteration with standard deviation. Data processing and reduction of hydrogen-deuterium exchange experiments utilized specialized DXMS data-reduction software (Sierra Analytics, Modesto, CA) (17,25, 26). Corrections for back exchange were determined via the methods of Zhang and Smith (38),

$$\text{Deuteration Level}\,(\%) = \frac{\text{m}\,(\text{P}) - \text{m}\,(\text{N})}{\text{m}\,(\text{F}) - \text{m}\,(\text{N})} \times 100$$

where m(P), m(N), and m(F) are the centroid value of partially deuterated peptide, nondeuterated peptide, and fully deuterated peptide, respectively.

Homology Modeling of SEX4

HHpred search (39,40) and InterPro domain scan (41) was used to determine which available structure of a DSP domain was the best template to model the DSP domain of SEX4. The top four hits of each search were aligned with the DSP domain of SEX4 using PROfile Multiple Alignment with predicted Local Structure 3D (PROMALS3D) (42). These alignments served as inputs for the alignment mode of SWISS-MODEL in Swiss PDB viewer version 8.05 (43) to generate a homology model of the SEX4 DSP domain. Each homology model was analyzed visually and by Anolea, Gromos, and Verify3d (44-46). The model utilizing VHR (Protein Data Bank code 1vhr) as the template was the best model.

RESULTS

Laforin and SEX4 are both composed of a carbohydrate binding module (CBM) and a dual specificity phosphatase (DSP) domain (Fig. 1A). In addition to these two domains, SEX4 also contains a chloroplast targeting peptide (cTP), to target it to the site of starch synthesis in plants. The CBM of laforin and SEX4 are 38% similar at the amino acid level (Fig. 1B) and while they belong to different CBM families, CBM20 and CBM21 respectively, they belong to the same evolutionarily related CBM clan (47-49). The AMP-activated kinase targeting subunit β1 (AMPKβ1) is also a member of this clan, shares 49% similarity with the SEX4 CBM, and is the closest homolog with a solved crystal structure and detailed knowledge of key residues that are necessary for glucan binding (50). The phosphatase domains of laforin and SEX4 are 33% similar (Fig. 1B). A BLASTp search of the non-redundant GenBank human database with the SEX4 DSP identifies laforin as the closest match (6e-07) and human Vaccinia virus H1-related (VHR) phosphatase as the one of the closest matches with a solved structure (2e-04). The DSP of SEX4 and VHR are 36% similar at the amino acid level (Fig. 1B). For these reasons, we utilized the structural information known about the CBM of AMPKβ1 and the DSP domain of VHR throughout our study.

Recombinant expression, purification, and biochemical characterization of Δ81-SEX4

We previously reported that full-length SEX4 is largely insoluble; however, deletion of the first fifty-two amino acids (Δ52-SEX4) yields soluble protein (11). We also previously demonstrated that recombinant Δ52-SEX4 binds carbohydrates, utilizes the exogenous phosphatase substrate *para*-nitrophenylphosphate (*p*-NPP), and has the unique activity of dephosphorylating phosphoglucans (11). This was the first extensive biochemical characterization of a glucan phosphatase that reported all three of these functions.

Truncation of the first fifty-two amino acids deletes some of the cTP of SEX4 (Fig. 2A). However, we felt this partial truncation of the cTP might interfere in our DXMS studies and therefore generated Δ81-SEX4 to eliminate the entire cTP (Fig. 2A). Before proceeding to DXMS studies, we first characterized Δ81-SEX4 to ensure it behaved like Δ52-SEX4. We found that Δ81-SEX4 has a lower specific activity than Δ52-SEX4 against *p*-NPP (Fig. 2B). While Δ81-SEX4 has a lower activity against the exogenous substrate *p*-NPP, it liberates phosphate from amylopectin to a greater extent than Δ52-SEX4 (Fig. 2C). Phosphatase activity by a DSP is dependent on a nucleophilic cysteine residue conserved in the DSP signature motif, HCxxGxxRS (51,52). Therefore we mutated this residue and, as expected, found that activity against phosphoglucans and *p*-NPP are both dependent on the catalytic cysteine (Fig. 2B and C). With respect to glucan binding, Δ81-SEX4 and Δ81-SEX4-C/S both bind amylopectin to similar degrees as previously observed for Δ52-SEX4 (Fig. 2D) (11).

As previously mentioned, the CBM of AMPKβ1 is closely related to the CBM of SEX4, and the AMPKβ1 CBM is structurally well defined. Polekhina and colleagues demonstrated which residues in the CBM of AMPKβ1 participate in glucan binding (50,53). Based on this work, we mutated residues predicted to participate in glucan binding of SEX4. As expected, these mutations abolished or greatly reduced glucan binding of Δ81-SEX4 (Fig. 2D). We reported for Δ52-SEX4 that inhibition of glucan binding also inhibited glucan phosphatase activity (11). Similar to Δ52-SEX4, mutation of glucan binding residue in Δ81-SEX4 also greatly reduced its glucan phosphatase activity, but did not affect *p*-NPP activity (Fig. 2B and C). Cumulatively, these data show that Δ81-SEX4 behaves in a similar manner as previously reported for Δ52-SEX4 and suggest that partial truncation of the cTP (Δ52-SEX4) may slightly inhibit the glucan phosphatase activity of SEX4.

Pepsin fragmentation and peptide identification of Δ81-SEX4-C/S

Mutation of a DSP nucleophilic cysteine to a serine inhibits substrate dephosphorylation, but allows the phosphatase to correctly position the substrate in the active site cleft (54,55). In addition, the Cys/Ser mutant binds substrates with similar affinities as the wild-type enzyme (56-58). Therefore, we utilized the catalytically inactive Δ81-SEX4-C/S in our DXMS analysis and purified it to greater than 95% homogeneity (Fig. 3A and Supplemental Fig. 1).

We first optimized the pepsin digestion and HPLC separation conditions of Δ81-SEX4-C/S so that we produced fragments of the appropriate size and distribution for exchange analysis. Optimal digestion was obtained by diluting 1.0 part of deuterated Δ81-SEX4-C/S with 1.3 parts of the quench solution and then exposed to immobilized pepsin for 16 s. These conditions resulted in the production and identification of 264 probe peptides covering 100% of the 307 amino acids of Δ81-SEX4-C/S. (Fig. 3B). Of these 264 peptides, we chose 28 peptides that covered the entire sequence to monitor in subsequent experiments.

H/D Exchange of Apo-Δ81-SEX4-C/S

We began our H/D exchange experiments using Δ81-SEX4-C/S in the absence of glucan (Apo-Δ81-SEX4-C/S). We incubated Δ81-SEX4-C/S in D_2O for 10 s to 10,000 s (166.67 min), quenched the reactions by rapidly lowering the pH and temperature, pepsin digested the sample, separated the peptides by HPLC, and analyzed the in-exchange rate of deuterium by electrospray ionization mass spectrometry.

Combining the H/D exchange data with the peptide map allows one to assess the level of deuteration for specific regions of the protein. In the Apo-Δ81-SEX4-C/S, the regions of the DSP domain that were highly accessible to solvent, defined as more than 50% deuterated after 300 s in D_2O, are regions predicted to be between β-sheets and α-helices in SEX4 (Fig. 4) and known to be in loops and turns in phosphatase crystal structures (reviewed in (51,59-61)). The only peptide that did not behave in this manner was peptide 79-88, the amino-terminal peptide. Peptide 79-88 is predicted to be an alpha-helix, but exhibited greater than 90% deuteration at the earliest time-point. This result is likely due to the fact that we truncated the first 80 amino acids of SEX4 and disrupted this predicted helix.

Within the DSP domain, the recognition domain, D-loop, PTP-loop, and the first half of the variable loop (amino acids 130-143) were all highly solvent accessible regions (Fig. 4). Within the CBM, two regions that contain residues known to coordinate glucan binding, 275-292 and 312-333, were highly accessible as were residues 334-360 and the carboxy-terminal tail (Fig. 4).

The highly accessible portions of the DSP domain fall within the active site (PTP-loop) and regions known to coordinate substrate presentation to the active site in other dual specificity phosphatases (i.e. the D-loop, recognition domain, and variable loop) (59-61). Within the CBM, four of the five residues (W278, W314, G329, and N333) known to coordinate glucan binding are within regions that are highly solvent accessible. The high levels of deuteration in these portions of the DSP domain and CBM are either predicted to be in exposed loops and/or bind the phosphoglucan.

Percent change in H/D exchange of Apo- versus amylopectin-bound-Δ81-SEX4-C/S

We then performed the same experiment as described above for Apo-Δ81-SEX4-C/S using Δ81-SEX4-C/S in the presence of the phosphoglucan amylopectin. Figure 5 shows the spectra results for one peptide (residues 312-333) from the CBM prior to exposure to D_2O (no D_2O), after exposure to D_2O in the absence of amylopectin (Apo), and after exposure to D_2O in the presence of amylopectin (+Amylopectin). Incorporation of deuterium is evident from the

increase in mass and complexity of the peaks as a function of deuteration time (Fig. 5A & B). When Δ81-SEX4-C/S binds amylopectin, the spectra undergoes a prominent leftward shift on the *m/z* axis, indicating a uniform decrease in deuteration when bound to amylopectin. This shift is in sharp contrast to spectra for Apo (Fig. 5B) and the fully deuterated peptide (Fig. 5D).

We investigated each of the 28 peptides from Figure 3 of Δ81-SEX4-C/S Apo and amylopectin bound in a similar manner as in Figure 5 to identify peptides that underwent increased, decreased, or no change in H/D exchange upon substrate binding. To compare the deuteration changes in Apo versus amylopectin-bound SEX4, we compared the percentage of deuteration in each peptide in the absence and presence of amylopectin. We identified fourteen peptides that displayed a greater than 10% change in percent deuteration in the presence of amylopectin during the 10,000 second experiment. For these fourteen peptides, we did not observed any increases in deuteration greater than 10%. Instead, all of the changes in percent deuteration were decreases. In the DSP domain, we identified eight peptides out of seventeen total that exhibited a considerable decrease (> 10% decrease) in deuteration in the presence of the glucan (Fig. 6 and Supplemental Fig. 2). In the CBM, we identified six peptides out of eight total that exhibited a substantial decrease in deuteration (Fig. 7 and Supplemental Fig. 3). We did not observe a change greater than 10% in percent deuteration in the peptides outside of these two domains (Supplemental Fig. 2 & 3).

To determine the position of these peptides within SEX4, we overlaid the H/D exchange rates onto the peptides that were analyzed by mass spectrometry (Fig. 4 and Supplemental Fig. 4) and graphed the maximum percent change as a positive (increase) or negative (decrease) change in deuteration (Fig. 8A). Since we observed no increase in deuteration greater than 10%, the percent changes shown in Figure 8A are percent decreases.

Within the CBM, peptides containing residues known to coordinate glucan binding all experienced decreased H/D exchange upon glucan addition (Fig. 8A, arrows). Poekhlina et al. showed that these residues in the CBM21 domain of AMPKβ1 subunit all contact the glucan (50, 53). In addition, we demonstrated that mutation of these residues in Δ81-SEX4 and Δ52-SEX4 reduces or abolishes glucan binding (Fig. 2D and (11)). Therefore, the decrease in H/D exchange of these residues suggests that they are performing the same function in Δ81-SEX4-C/S, i.e. binding the glucan. In addition to these regions of the CBM, residues 260-275 and 293-304 also undergo a >20% and >30%, respectively, reduction in deuteration upon amylopectin binding (Fig. 7A and Fig. 8A). While residues in this region of the CBM are not known to be necessary for glucan binding, these peptides encompass β-sheets in the AMPKβ1 structure that are in close proximity to the substrate and are predicted to be located in analogous β-sheets in the SEX4 CBM (Supplemental Fig. 5) (50). Thus, our data suggest these regions in SEX4 are in contact with the glucan.

While the H/D exchange data from the CBM confirms known aspects of CBM-glucan binding, the exchange data from the DSP domain is most insightful. The four regions that coordinate substrate presentation to the active site of phosphatases are the recognition domain (residues 89-99), variable loop (residues 130-161), D-loop (residues 163-171), and PTP loop (residues 196-204) (59). Strikingly, these regions all undergo a dramatic decrease in H/D exchange upon glucan binding (Fig. 6 and Fig. 8A). Since we did not observe any substantial increases in deuteration, these data strongly suggest an extensive interaction between these regions and the glucan and suggest that they are presenting the phosphoglucan to the active site. The interaction with the glucan then provides protection from deuteration for these regions.

In addition to peptides covering the above four DSP regions, we also observed a significant decrease in deuteration in peptides 106-111 and 172-176 (Fig. 6). Peptide 106-111 is predicted to be in a loop region between the delta-like domain and variable loop (Fig. 4). Peptide 172-176

is within α-helix four of the DSP just prior to the PTP loop (Fig. 4). These regions have not been identified as playing a role in DSP substrate binding; however, to our knowledge it has not been investigated whether analogous regions play a role in substrate binding in other DSPs. Thus, it is entirely possible that these two regions interact with the phosphoglucan and as we discuss in subsequent sections our data suggest that they are in a position to do so.

Since amylopectin is a heterogeneous polymer, we decided to perform a similar set of experiments using the homogenous, seven-ringed, cyclic oligosaccharide β-cyclodextrin. These experiments also identified the peptides within the CBM that contain the five known residues that coordinate glucan binding and amino acids 261-275 as regions protected from H/D exchange (Fig. 8B). The largest change within the CBM was in peptide 305-313, yielding an approximate 20% greater decrease compared to amylopectin (Fig. 8). Based on the crystal structure of the AMPKβ CBM (the closest CBM homolog with a solved structure), peptide 305-313 of SEX4 contains a glycine (G329) and aspargine (N333) that are predicted to make direct contact with β-cyclodextrin. Since β-cyclodextrin is much more homogeneous than amylopectin, the 20% greater decrease is likely the result of a higher percent of β-cyclodextrin making contact with these residues and/or making more extensive contact with them.

The results in the DSP domain in the presence of β-cyclodextrin were not as dramatic as observed with amylopectin, but β-cyclodextrin showed a similar pattern of protection as amylopectin with the highest degree of protection in the variable-loop (Fig. 8B). This less robust result is likely due to the markedly smaller size β-cyclodextrin compared to amylopectin. Cumulatively, these data strongly support our previous finding that SEX4 is a glucan phosphatase and yield insights into the mechanistic action of this activity.

Modeled analysis of the SEX4 DSP domain

To better interrupt the predicted changes in the SEX4 DSP domain upon glucan binding, we generated a homology model of this region. As previously mentioned, a BLASTp search of the SEX4 DSP identifies laforin as the closest match (6e-07) and VHR as one of the closest matches with a solved structure (2e-04). In addition, the DSP of SEX4 and VHR are 35% similar at the amino acid level (Fig. 1B). To identify the most appropriate crystal structure to utilize in our modeling efforts, we analyzed the sequence of the SEX4 DSP domain using HHpred search (39,40) and InterPro domain scan (41), both of which query alignment and structural databases, such as Pfam, SMART, PDB, CDD, and HMMTigr, using hidden Markov models. InterPro domain scan identified human VHR as the highest hit (3.3E-37) and HHpred identified VHR as one of the highest hits (7.2E-37). To confirm these results, we compared the predicted secondary structure of the SEX4 DSP domain with the known secondary structure of human VHR. The DSP domains of SEX4 and VHR share very similar predicted secondary structure (Fig. 9A).

Because no crystal structure is available for a glucan phosphatase, we utilized the above results to generate a homology model of the SEX4 DSP using the SWISS-MODEL function in Swiss PDB viewer (43). We first generated a sequence alignment of the DSP domains of SEX4 and VHR using PROfile Multiple Alignment with predicted Local Structure 3D (PROMALS3D), which utilizes primary, predicted secondary, and available tertiary information to align sequences (42). We then utilized the crystal structure of VHR to generate a homology model of the DSP domain of SEX4.

To gain insights into the spatial arrangement of our DXMS results, we overlaid the percent change in deuteration onto the structural model (Fig. 9B). The regions of the SEX4 DSP that undergo a dramatic decrease in deuteration upon glucan binding are the D-loop, recognition domain, variable loop, PTP loop, peptide 106-111, and peptide 172-176 (Fig. 9B). The D-loop contains the aspartate that functions as the general acid-base catalyst in the dephosphorylation

reaction and thus makes direct contact with the phosphorylated substrate (52). Saper and colleagues originally demonstrated that the recognition domain contributes to the depth of the active site and that it is also involved in substrate binding, aspects seen in other phosphatase structures as well (52,55,62,63). The variable loop assists in orienting the active site arginine to interact with the phosphate of the substrate and is in close proximity to the substrate (52, 59). Within the PTP loop, multiple residues participate in presenting the phosphosubstrate to the active site and/or are involved in forming a phophoenzyme intermediate with the substrate (51,52,59). Our homology model predicts that peptides 106-111 and 172-176 are positioned close to and on opposite sides of the active site. Thus, all of the regions of the DSP domain that undergo a dramatic decrease in deuteration are the four regions that are involved in presenting the phospho-substrate to the active site and two regions that we predict are in close proximity to the active site. This conclusion is supported by a surface view of the SEX4 DSP domain model (Fig. 9C). This view demonstrates that these regions envelope the active site (shown in red) and are concentrated around the active site.

The region demonstrating a decrease in deuteration on the opposite face of the DSP domain corresponds to Tyr^{184}-Gly^{191} (Fig. 9C, inset). The exchange data for these amino acids are on the same peptide as the PTP loop, peptide 184-209 (Fig. 3B). Thus, the resolution in this region is decreased compared with the majority of our data. We attempted to obtain peptides that separated the PTP loop from these amino acids, but were unable to do so. Nonetheless, we predict that residues 184-191 likely do not interact with the phosphoglucan and are highlighted due to the interaction between the PTP loop residues and amylopectin.

DISCUSSION

To date, there have been no mechanistic or structural studies on the newly described glucan phosphatases. We utilized DXMS to determine how the two domains of one glucan phosphatase, SEX4, behave upon phosphoglucan binding. Our data suggest that SEX4 does not undergo a large-scale rearrangement upon glucan binding. Instead, our results suggest only minor rearrangement of the CBM and DSP domain upon glucan binding. Within the CBM, our data confirmed that peptides containing residues known to coordinate glucan binding perform a similar function in SEX4. While these results were as expected, the results we obtained concerning the DSP domain of SEX4 were quite insightful. These data identified regions within the SEX4 DSP domain and adjacent to the active site that intimately interact with the phosphoglucan, including the recognition domain, D-loop, variable loop, and PTP loop.

Changes that occur early in H/D exchange time course experiments are most often the result of differences in solvent accessibility caused by direct interaction of the peptide with the substrate and/or a conformational alteration in the protein upon substrate binding. Significant conformational alterations cause new residues to be exposed and others to be more protected, as is the case with Factor VIIa, Epac, the cytosolic group IVA phospholipase A_2, eIF4E, and ERK2 (37,64-67). Since Δ81-SEX4-C/S only undergoes decreased deuteration, the decreased deuteration occur early in the experiment, and it lacks increased deuteration, these data collectively argue that upon glucan binding there is no large-scale rearrangement of the CBM or DSP domain. It also suggests that there is not a sub-domain conformational change that is then propagated throughout the domain or the protein, as this action would cause both increased and decreased deuteration. Even upon extending the timeframe of our analysis by 100 fold, we only observed data suggestive of a local conformational change in one peptide, peptide 99-105 (data not shown). Instead, the data suggest that the regions undergoing decreased deuteration within both the CBM and DSP are being protected by the glucan itself.

Prior to this study, we envisioned three scenarios regarding the domain dynamics of the CBM and DSP domain of SEX4 (Fig. 10). The first two scenarios, depicted in Figure 10A and B, would each result in substantial domain rearrangement. Therefore, each of these cases would cause both an increase and decrease in the percent deuteration of the SEX4 CBM and DSP domain upon glucan binding. Since we did not observe an increase in the percent deuteration, our results indicate that SEX4 does not undergo a large-scale rearrangement upon glucan binding. Thus, our results suggest there is limited structural changes in SEX4 upon glucan binding (Fig. 10C) and eliminate models depicting global structural changes (Fig. 10A and B).

Another major finding of this study is the result suggesting that the DSP domain itself makes extensive and intimate contact with the phosphoglucan. The extensive interaction between the DSP and amylopectin, and to a similar extent with β-cyclodextrin, is surprising, but not without some precedent. Myotubularin-related protein-2 (MTMR2) binds and dephosphorylates specific phosphoinositols (60,68-71). One region of the DSP domain of MTMR2 undergoes a similar 25% decrease upon binding phosphatidylinositol 3-phosphate in a region that forms an extension to the active site pocket (68). Multiple regions of the DSP domain of SEX4 interact with phosphoglucans in a similar manner as seen with the one region of MTMR2 and phosphoinositols, but the SEX4 DSP interacts with the phosphoglucan to a more extensive degree than was observed with MTMR2 and phosphatidylinositol 3-phosphate. The regions of the SEX4 DSP domain that interact with amylopectin are the recognition domain, D-loop, variable loop, PTP loop, peptide 106-111, and peptide 172-176. Our homology model predicts that each region is located on the same surface as the active site and that these regions engulf the SEX4 active site. Thus, they are located in a manner to interact with and present the phosphoglucan to the active site.

Our analyses also identified that the variable loop of SEX4 is atypical compared to other dual specificity phosphatases (DSPs). The variable loop of most DSPs is shorter than the variable loop of protein tyrosine specific phosphatases (PTPs). This difference is due to the need for a deeper active site in PTPs to accommodate the longer head group of a phospho-Tyr versus the shorter phospho-Ser/Thr. The deeper active site of PTPs largely accounts for their Tyr specificity, since P-Ser or P-Thr are essentially too short to reach the active site of PTPs. Interestingly, the variable loop of SEX4 is 25-50% longer than most DSPs, including the prototypical dual specificity phosphatase VHR (Fig. 9A). This increased length predicts that SEX4 likely has a deeper active site than DSPs that dephosphorylate phospho-proteinaceous substrates. Many of the DSPs that dephosphorylate non-proteinaceous substrates, e.g. PTEN and the myotubularins, have a deep and wide catalytic pocket to accommodate the phosphorylated inositol ring (60,68,72). Since SEX4 and laforin have a longer variable loop than dual specificity phosphatases that act on proteinaceous substrates, we predict that the active site of glucan phosphatases will be deeper and wider than these phosphatases; and more closely resemble that of phosphatases that dephosphorylate non-proteinaceous substrates.

In summary, our data support a model whereby the DSP domain and CBM of SEX4 intimately interact with glucans and one whereby the domains do not undergo global rearrangement upon glucan binding. The interactions between the SEX4 CBM and the glucan is as expected since carbohydrate binding modules by definition bind carbohydrates. However, the extensive interaction between the DSP domain and glucan is both surprising and insightful. Collectively, our results strengthen the case that SEX4 and, by inference, laforin are glucan phosphatases and provide the first structural insights into the dynamics of the CBM and DSP domain upon glucan binding.

Supplementary Material

Refer to Web version on PubMed Central for supplementary material.

Acknowledgments

We thank Drs. Craig Vander Kooi and Doug Andres for fruitful discussions regarding these data.

Funding: This work was supported by National Institutes of Health grants 5R00NS061803, 5P20RR0202171, and University of Kentucky College of Medicine startup funds (to M.S.G.); the Korea Research Foundation grant KRF-2008-331-E00031 (to Y.J.K); and Innovative Technologies for the Molecular Analysis of Cancer (IMAT) program (CA099835, and CA118595, V.L.W.), NIH Grants AI076961, AI081982, AI2008031, AI072106, AI068730, GM037684, GM020501, GM066170, (V.L.W.), and a Discovery Grant (UC10591) from the University of California IUCRP Program, BiogenIDEC corporate sponsor (to V.L.W.).

Abbreviations

AMPKβ1, AMP-activated kinase targeting subunit β1
CBM, carbohydrate binding module
cTP, chloroplast targeting peptide
DSP, dual specificity phosphatase
DTT, dithiothreitol
DXMS, deuterium exchange mass spectrometry
GuHCL, Guanidine hydrochloride
GWD, glucan water dikinase
LD, Lafora disease
LB, Lafora body
MTMR2, Myotubularin-related protein-2
p-NPP, para-nitrophenylphosphate
PROMALS3D, profile multiple alignment with predicted local structure 3D
PTPs, protein tyrosine specific phosphatases
PWD, phosphoglucan water dinkinase
SEX4, starch excess 4
VHR, Vaccinia virus H1-related

REFERENCES

1. Hoof FV, Hageman-Bal M. Progressive familial myoclonic epilepsy with lafora bodies. Acta Neuropathologica 1967;V7:315–326. [PubMed: 4166286]
2. Lafora GR, Gluck B. Beitrag zur histopathologie der myoklonischen epilepsie. Z Ges Neurol Psychiatr 1911;6:1–14.
3. Collins GH, Cowden RR, Nevis AH. Myoclonus epilepsy with Lafora bodies. An ultrastruc- tural and cytochemical study. Arch Pathol 1968;86:239–254. [PubMed: 4877594]
4. Lafora GR. Uber des Vorkommen amyloider KJrperchen im innern der Ganglienzellen. Virchows Arch. f. Path. Anat 1911;205:295.
5. Sakai M, Austin J, Witmer F, Trueb L. Studies in myoclonus epilepsy (Lafora body form). II. Polyglucosans in the systemic deposits of myoclonus epilepsy and in corpora amylacea. Neurology 1970;20:160–176. [PubMed: 4188951]
6. Yokoi S, Austin J, Witmer F. Isolation and characterization of Lafora bodies in two cases of myoclonus epilepsy. Journal of Neuropathology and Experimental Neurology 1967;26:125–127. [PubMed: 4164450]
7. Yokoi S, Austin J, Witmer F, Sakai M. Studies in myoclonus epilepsy (Lafora body form). I. Isolation and preliminary characterization of Lafora bodies in two cases. Arch Neurol 1968;19:15–33. [PubMed: 4175641]
8. Minassian BA, Lee JR, Herbrick JA, Huizenga J, Soder S, Mungall AJ, Dunham I, Gardner R, Fong CY, Carpenter S, Jardim L, Satishchandra P, Andermann E, Snead OC 3rd, Lopes-Cendes I, Tsui LC, Delgado-Escueta AV, Rouleau GA, Scherer SW. Mutations in a gene encoding a novel protein tyrosine phosphatase cause progressive myoclonus epilepsy. Nat Genet 1998;20:171–174. [PubMed: 9771710]

9. Serratosa JM, Gomez-Garre P, Gallardo ME, Anta B, de Bernabe DB, Lindhout D, Augustijn PB, Tassinari CA, Malafosse RM, Topcu M, Grid D, Dravet C, Berkovic SF, de Cordoba SR. A novel protein tyrosine phosphatase gene is mutated in progressive myoclonus epilepsy of the Lafora type (EPM2). Hum Mol Genet 1999;8:345–352. [PubMed: 9931343]
10. Wang J, Stuckey JA, Wishart MJ, Dixon JE. A unique carbohydrate binding domain targets the lafora disease phosphatase to glycogen. J Biol Chem 2002;277:2377–2380. [PubMed: 11739371]
11. Gentry MS, Dowen RH 3rd, Worby CA, Mattoo S, Ecker JR, Dixon JE. The phosphatase laforin crosses evolutionary boundaries and links carbohydrate metabolism to neuronal disease. J Cell Biol 2007;178:477–488. [PubMed: 17646401]
12. Worby CA, Gentry MS, Dixon JE. Laforin: A dual specificity phosphatase that dephosphorylates complex carbohydrates. J. Biol. Chem 2006;281:30412–30418. [PubMed: 16901901]
13. Tagliabracci VS, Girard JM, Segvich D, Meyer C, Turnbull J, Zhao X, Minassian BA, Depaoli-Roach AA, Roach PJ. Abnormal metabolism of glycogen phosphate as a cause for lafora disease. J Biol Chem. 2008
14. Tagliabracci VS, Turnbull J, Wang W, Girard JM, Zhao X, Skurat AV, Delgado-Escueta AV, Minassian BA, Depaoli-Roach AA, Roach PJ. Laforin is a glycogen phosphatase, deficiency of which leads to elevated phosphorylation of glycogen in vivo. Proc Natl Acad Sci U S A 2007;104:19262–19266. [PubMed: 18040046]
15. Solaz-Fuster MC, Gimeno-Alcaniz JV, Ros S, Fernandez-Sanchez ME, Garcia-Fojeda B, Criado Garcia O, Vilchez D, Dominguez J, Garcia-Rocha M, Sanchez-Piris M, Aguado C, Knecht E, Serratosa J, Guinovart JJ, Sanz P, Rodriguez de Cordoba S. Regulation of glycogen synthesis by the laforin-malin complex is modulated by the AMP-activated protein kinase pathway. Hum Mol Genet 2008;17:667–678. [PubMed: 18029386]
16. Vilchez D, Ros S, Cifuentes D, Pujadas L, Valles J, Garcia-Fojeda B, Criado-Garcia O, Fernandez-Sanchez E, Medrano-Fernandez I, Dominguez J, Garcia-Rocha M, Soriano E, Rodriguez de Cordoba S, Guinovart JJ. Mechanism suppressing glycogen synthesis in neurons and its demise in progressive myoclonus epilepsy. Nat Neurosci 2007;10:1407–1413. [PubMed: 17952067]
17. Worby CA, Gentry MS, Dixon JE. Malin decreases glycogen accumulation by promoting the degradation of protein targeting to glycogen (PTG). J Biol Chem 2008;283:4069–4076. [PubMed: 18070875]
18. Gentry MS, Pace RM. Conservation of the glucan phosphatase laforin is linked to rates of molecular evolution and the glycogen metabolism of the organism. BMC Evol Biol 2009;9:138. [PubMed: 19545434]
19. Niittyla T, Comparot-Moss S, Lue W-L, Messerli G, Trevisan M, Seymour MDJ, Gatehouse JA, Villadsen D, Smith SM, Chen J, Zeeman SC, Smith AM. Similar protein phosphatases control starch metabolism in plants and glycogen metabolism in mammals. J. Biol. Chem 2006;281:11815–11818. [PubMed: 16513634]
20. Sokolov LN, Dominguez-Solis JR, Allary AL, Buchanan BB, Luan S. A redox-regulated chloroplast protein phosphatase binds to starch diurnally and functions in its accumulation. Proc Natl Acad Sci U S A 2006;103:9732–9737. [PubMed: 16772378]
21. Kerk D, Conley TR, Rodriguez FA, Tran HT, Nimick M, Muench DG, Moorhead GB. A chloroplast-localized dual-specificity protein phosphatase in Arabidopsis contains a phylogenetically dispersed and ancient carbohydrate-binding domain, which binds the polysaccharide starch. Plant J 2006;46:400–413. [PubMed: 16623901]
22. Kotting O, Santelia D, Edner C, Eicke S, Marthaler T, Gentry MS, Comparot-Moss S, Chen J, Smith AM, Steup M, Ritte G, Zeeman SC. STARCH-EXCESS4 Is a Laforin-Like Phosphoglucan Phosphatase Required for Starch Degradation in Arabidopsis thaliana. Plant Cell 2009;21:334–346. [PubMed: 19141707]
23. Smith AM, Zeeman SC, Smith SM. Starch degradation. Annual Review of Plant Biology 2005;56:73–98.
24. Zeeman SC, Smith SM, Smith AM. The diurnal metabolism of leaf starch. Biochemical Journal 2007;401:13–28. [PubMed: 17150041]
25. Blennow A, Nielsen TH, Baunsgaard L, Mikkelsen R, Engelsen SB. Starch phosphorylation: a new front line in starch research. Trends Plant Sci 2002;7:445–450. [PubMed: 12399179]

26. Hejazi M, Fettke J, Haebel S, Edner C, Paris O, Frohberg C, Steup M, Ritte G. Glucan, water dikinase phosphorylates crystalline maltodextrins and thereby initiates solubilization. Plant J 2008;55:323–334. [PubMed: 18419779]
27. Hvidt A, Nielsen SO. Hydrogen exchange in proteins. Adv Protein Chem 1966;21:287–386. [PubMed: 5333290]
28. Linderstrom-Lang, KU. Deuterium exchange and protein structure. Methuen; London: 1958.
29. Busenlehner LS, Armstrong RN. Insights into enzyme structure and dynamics elucidated by amide H/D exchange mass spectrometry. Arch Biochem Biophys 2005;433:34–46. [PubMed: 15581564]
30. Hoofnagle AN, Resing KA, Ahn NG. Protein analysis by hydrogen exchange mass spectrometry. Annu Rev Biophys Biomol Struct 2003;32:1–25. [PubMed: 12598366]
31. Tsutsui Y, Wintrode PL. Hydrogen/deuterium exchange-mass spectrometry: a powerful tool for probing protein structure, dynamics and interactions. Curr Med Chem 2007;14:2344–2358. [PubMed: 17896983]
32. Gentry MS, Worby CA, Dixon JE. Insights into Lafora disease: malin is an E3 ubiquitin ligase that ubiquitinates and promotes the degradation of laforin. Proc Natl Acad Sci U S A 2005;102:8501–8506. [PubMed: 15930137]
33. Burns-Hamuro LL, Hamuro Y, Kim JS, Sigala P, Fayos R, Stranz DD, Jennings PA, Taylor SS, Woods VL Jr. Distinct interaction modes of an AKAP bound to two regulatory subunit isoforms of protein kinase A revealed by amide hydrogen/deuterium exchange. Protein Sci 2005;14:2982–2992. [PubMed: 16260760]
34. Hamuro Y, Anand GS, Kim JS, Juliano C, Stranz DD, Taylor SS, Woods VL Jr. Mapping intersubunit interactions of the regulatory subunit (RIalpha) in the type I holoenzyme of protein kinase A by amide hydrogen/deuterium exchange mass spectrometry (DXMS). J Mol Biol 2004;340:1185–1196. [PubMed: 15236976]
35. Pantazatos D, Kim JS, Klock HE, Stevens RC, Wilson IA, Lesley SA, Woods VL Jr. Rapid refinement of crystallographic protein construct definition employing enhanced hydrogen/deuterium exchange MS. Proc Natl Acad Sci U S A 2004;101:751–756. [PubMed: 14715906]
36. Spraggon G, Pantazatos D, Klock HE, Wilson IA, Woods VL Jr. Lesley SA. On the use of DXMS to produce more crystallizable proteins: structures of the T. maritima proteins TM0160 and TM1171. Protein Sci 2004;13:3187–3199. [PubMed: 15557262]
37. Brock M, Fan F, Mei FC, Li S, Gessner C, Woods VL Jr. Cheng X. Conformational analysis of Epac activation using amide hydrogen/deuterium exchange mass spectrometry. J Biol Chem 2007;282:32256–32263. [PubMed: 17785454]
38. Zhang Z, Smith DL. Determination of amide hydrogen exchange by mass spectrometry: a new tool for protein structure elucidation. Protein Sci 1993;2:522–531. [PubMed: 8390883]
39. Soding J. Protein homology detection by HMM-HMM comparison. Bioinformatics 2005;21:951–960. [PubMed: 15531603]
40. Soding J, Biegert A, Lupas AN. The HHpred interactive server for protein homology detection and structure prediction. Nucleic Acids Res 2005;33:W244–248. [PubMed: 15980461]
41. Zdobnov EM, Apweiler R. InterProScan--an integration platform for the signature-recognition methods in InterPro. Bioinformatics 2001;17:847–848. [PubMed: 11590104]
42. Pei J, Kim BH, Grishin NV. PROMALS3D: a tool for multiple protein sequence and structure alignments. Nucleic Acids Res 2008;36:2295–2300. [PubMed: 18287115]
43. Arnold K, Bordoli L, Kopp J, Schwede T. The SWISS-MODEL workspace: a web-based environment for protein structure homology modelling. Bioinformatics 2006;22:195–201. [PubMed: 16301204]
44. Melo F, Devos D, Depiereux E, Feytmans E. ANOLEA: a www server to assess protein structures. Proc Int Conf Intell Syst Mol Biol 1997;5:187–190. [PubMed: 9322034]
45. Luthy R, Bowie JU, Eisenberg D. Assessment of protein models with three-dimensional profiles. Nature 1992;356:83–85. [PubMed: 1538787]
46. Christen M, Hunenberger PH, Bakowies D, Baron R, Burgi R, Geerke DP, Heinz TN, Kastenholz MA, Krautler V, Oostenbrink C, Peter C, Trzesniak D, van Gunsteren WF. The GROMOS software for biomolecular simulation: GROMOS05. J Comput Chem 2005;26:1719–1751. [PubMed: 16211540]

47. Coutinho, PM.; Henrissat, B. Carbohydrate-active enzymes: an integrated database approach. In: Gilbert, HJ.; D., G.; Henrissat, B.; Svensson, B., editors. Recent Advances in Carbohydrate Bioengineering. The Royal Society of Chemistry; Cambridge: 1999. p. 3-12.
48. Machovic M, Janecek S. Starch-binding domains in the post-genome era. Cell Mol Life Sci 2006;63:2710–2724. [PubMed: 17013558]
49. Cantarel BL, Coutinho PM, Rancurel C, Bernard T, Lombard V, Henrissat B. The Carbohydrate-Active EnZymes database (CAZy): an expert resource for Glycogenomics. Nucleic Acids Res 2009;37:D233–238. [PubMed: 18838391]
50. Polekhina G, Gupta A, van Denderen BJ, Feil SC, Kemp BE, Stapleton D, Parker MW. Structural basis for glycogen recognition by AMP-activated protein kinase. Structure 2005;13:1453–1462. [PubMed: 16216577]
51. Denu JM, Stuckey JA, Saper MA, Dixon JE. Form and Function in Protein Dephosphorylation. Cell 1996;87:361. [PubMed: 8898189]
52. Yuvaniyama J, Denu JM, Dixon JE, Saper MA. Crystal structure of the dual specificity protein phosphatase VHR. Science 1996;272:1328–1331. [PubMed: 8650541]
53. Polekhina G, Gupta A, Michell BJ, van Denderen B, Murthy S, Feil SC, Jennings IG, Campbell DJ, Witters LA, Parker MW, Kemp BE, Stapleton D. AMPK beta subunit targets metabolic stress sensing to glycogen. Curr Biol 2003;13:867–871. [PubMed: 12747837]
54. Zhou B, Wu L, Shen K, Zhang J, Lawrence DS, Zhang ZY. Multiple regions of MAP kinase phosphatase 3 are involved in its recognition and activation by ERK2. J Biol Chem 2001;276:6506–6515. [PubMed: 11104775]
55. Jia Z, Barford D, Flint AJ, Tonks NK. Structural basis for phosphotyrosine peptide recognition by protein tyrosine phosphatase 1B. Science 1995;268:1754–1758. [PubMed: 7540771]
56. Wang F, Li W, Emmett MR, Hendrickson CL, Marshall AG, Zhang YL, Wu L, Zhang ZY. Conformational and dynamic changes of Yersinia protein tyrosine phosphatase induced by ligand binding and active site mutation and revealed by H/D exchange and electrospray ionization Fourier transform ion cyclotron resonance mass spectrometry. Biochemistry 1998;37:15289–15299. [PubMed: 9799489]
57. Xie L, Zhang YL, Zhang ZY. Design and characterization of an improved protein tyrosine phosphatase substrate-trapping mutant. Biochemistry 2002;41:4032–4039. [PubMed: 11900546]
58. Zhang YL, Yao ZJ, Sarmiento M, Wu L, Burke TR Jr. Zhang ZY. Thermodynamic study of ligand binding to protein-tyrosine phosphatase 1B and its substrate-trapping mutants. J Biol Chem 2000;275:34205–34212. [PubMed: 10952978]
59. Alonso, A.; Rojas, A.; Godzik, A.; Mustelin, T. The dual-specific protein tyrosine phosphatase family. Vol. 5. Springer; Berlin: 2003.
60. Begley MJ, Dixon JE. The structure and regulation of myotubularin phosphatases. Current Opinion in Structural Biology 2005;15:614–620. [PubMed: 16289848]
61. Andersen JN, Mortensen OH, Peters GH, Drake PG, Iversen LF, Olsen OH, Jansen PG, Andersen HS, Tonks NK, Moller NP. Structural and evolutionary relationships among protein tyrosine phosphatase domains. Mol Cell Biol 2001;21:7117–7136. [PubMed: 11585896]
62. Barford D, Flint AJ, Tonks NK. Crystal structure of human protein tyrosine phosphatase 1B. Science 1994;263:1397–1404. [PubMed: 8128219]
63. Stuckey JA, Schubert HL, Fauman EB, Zhang ZY, Dixon JE, Saper MA. Crystal structure of Yersinia protein tyrosine phosphatase at 2.5 A and the complex with tungstate. Nature 1994;370:571–575. [PubMed: 8052312]
64. Hsu YH, Burke JE, Stephens DL, Deems RA, Li S, Asmus KM, Woods VL Jr. Dennis EA. Calcium binding rigidifies the C2 domain and the intradomain interaction of GIVA phospholipase A2 as revealed by hydrogen/deuterium exchange mass spectrometry. J Biol Chem 2008;283:9820–9827. [PubMed: 18211893]
65. Rand KD, Andersen MD, Olsen OH, Jorgensen TJ, Ostergaard H, Jensen ON, Stennicke HR, Persson E. The origins of enhanced activity in factor VIIa analogs and the interplay between key allosteric sites revealed by hydrogen exchange mass spectrometry. J Biol Chem 2008;283:13378–13387. [PubMed: 18343822]

66. Zhou B, Zhang J, Liu S, Reddy S, Wang F, Zhang ZY. Mapping ERK2-MKP3 binding interfaces by hydrogen/deuterium exchange mass spectrometry. J Biol Chem 2006;281:38834–38844. [PubMed: 17046812]

67. Rutkowska-Wlodarczyk I, Stepinski J, Dadlez M, Darzynkiewicz E, Stolarski R, Niedzwiecka A. Structural changes of eIF4E upon binding to the mRNA 5′ monomethylguanosine and trimethylguanosine Cap. Biochemistry 2008;47:2710–2720. [PubMed: 18220364]

68. Begley MJ, Taylor GS, Brock MA, Ghosh P, Woods VL, Dixon JE. Molecular basis for substrate recognition by MTMR2, a myotubularin family phosphoinositide phosphatase. Proc Natl Acad Sci U S A 2006;103:927–932. [PubMed: 16410353]

69. Begley MJ, Taylor GS, Kim SA, Veine DM, Dixon JE, Stuckey JA. Crystal structure of a phosphoinositide phosphatase, MTMR2: insights into myotubular myopathy and Charcot-Marie-Tooth syndrome. Mol Cell 2003;12:1391–1402. [PubMed: 14690594]

70. Robinson FL, Dixon JE. Myotubularin phosphatases: policing 3-phosphoinositides. Trends Cell Biol 2006;16:403–412. [PubMed: 16828287]

71. Taylor GS, Maehama T, Dixon JE. Inaugural article: myotubularin, a protein tyrosine phosphatase mutated in myotubular myopathy, dephosphorylates the lipid second messenger, phosphatidylinositol 3-phosphate. Proc Natl Acad Sci U S A 2000;97:8910–8915. [PubMed: 10900271]

72. Lee J-O, Yang H, Georgescu M-M, Di Cristofano A, Maehama T, Shi Y, Dixon JE, Pandolfi P, Pavletich NP. Crystal Structure of the PTEN Tumor Suppressor: Implications for Its Phosphoinositide Phosphatase Activity and Membrane Association. Cell 1999;99:323–334. [PubMed: 10555148]

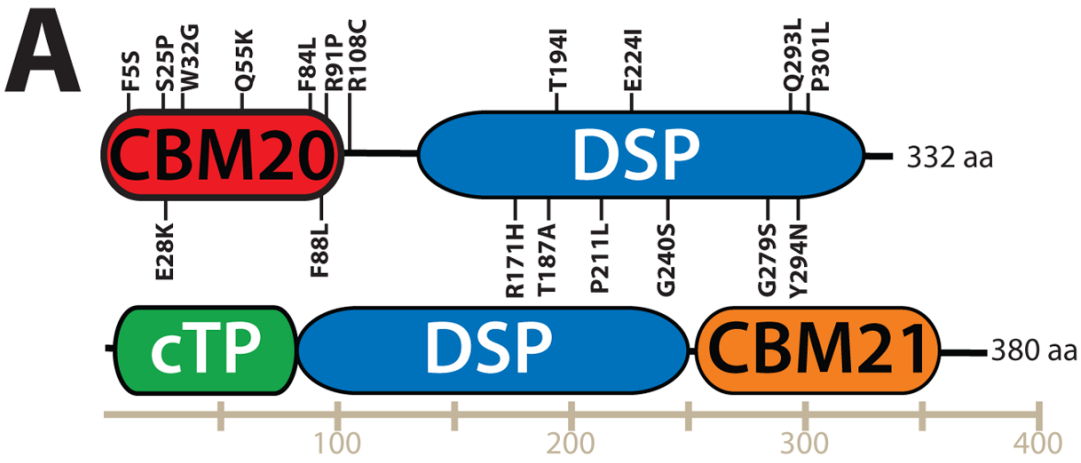

B

Percent Similarity/Identity

	SEX4	CBM	DSP
Hs-laforin	33/19	38/22	27/18
Hs-VHR			36/20
Hs-AMPKβ1		49/27	

FIGURE 1. Laforin and SEX4 domain structure and similarity of SEX4 with other CBM and DSP domains

A, Laforin is composed of a carbohydrate binding module, family 20 (CBM20), a linker region, and a dual specificity phosphatase (DSP) domain. LD patient nonsense mutations are shown. SEX4 contains a chloroplast targeting peptide (cTP), a DSP, and a carbohydrate binding module, family 21 (CBM21). *B*, Percent similarity and identity of full-length SEX4 and both domains compared with those of *H. sapiens*-laforin (Hs-laforin), -VHR (Hs-VHR), and -AMPKβ1 (Hs-AMPKβ1).

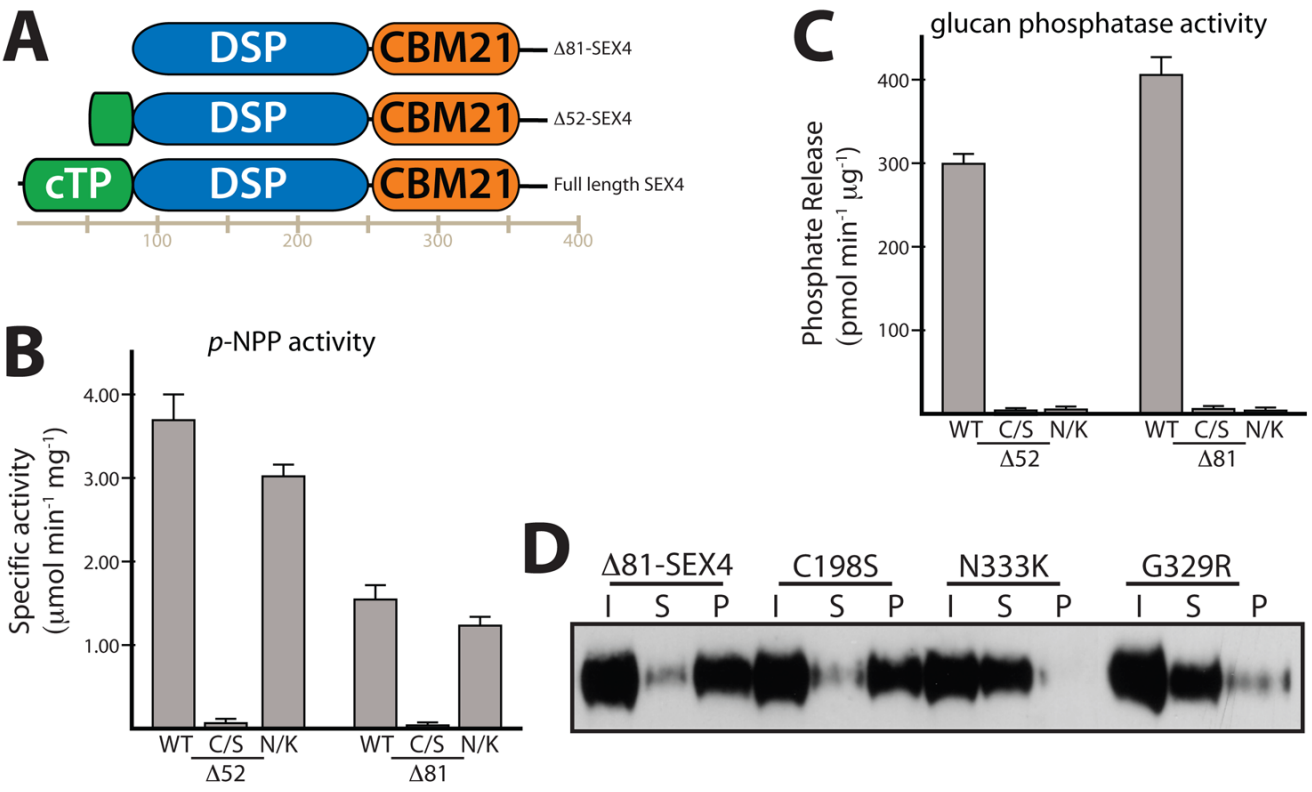

FIGURE 2. Biochemical characterization of SEX4 truncations

A, Schematic of SEX4 recombinant proteins used in this study: full length, amino terminal truncation of 52 amino acids (Δ52-SEX4), and amino terminal truncation of 81 amino acids (Δ81-SEX4). The schematic is to scale. cTP, chloroplast Targeting Peptide; DSP, dual specificity phosphatase domain; CBM, carbohydrate binding module. *B*, Specific activity of Δ52-SEX4 and Δ81-SEX4 against *para*-nitrophenylphosphate (*p*-NPP). WT, wild-type; C/S, C198S; N/K, N333K. *C*, Phosphate release from amylopectin by malachite green assays using Δ52-SEX4 and Δ81-SEX4 and mutants as in *B*. (*A* and *B*) Error bars indicate mean ± SD. *D*, Δ81-SEX4 recombinant histidine-tagged protein, input (I), was incubated with 5 mg/ml of amylopectin, amylopectin was pelleted by ultracentrifugation, and proteins in the input (I), pellet (P), and supernatant (S) were visualized by Western analysis as described. Mutated residues are designated with an asterisk in Figure 4 and highlighted in Supplemental Figure 5.

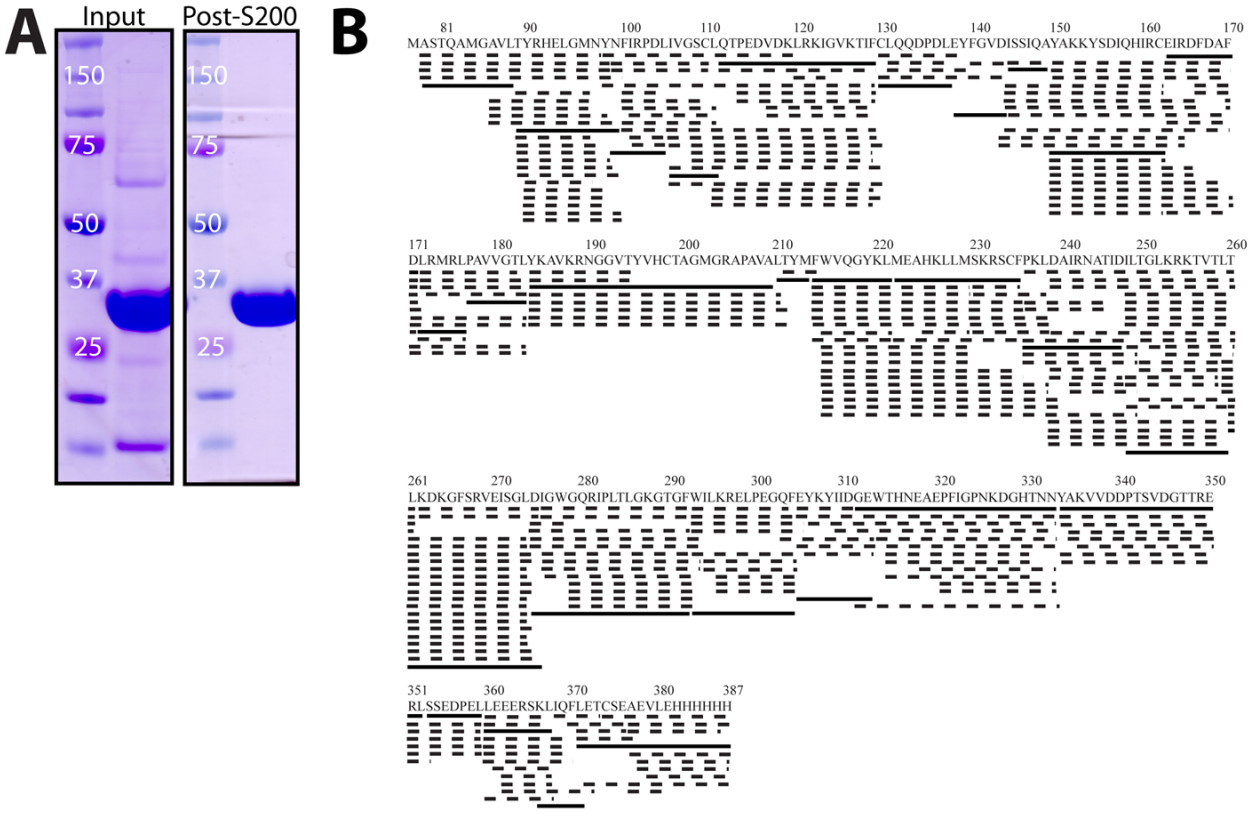

FIGURE 3. Purified recombinant protein and pepsin-digested coverage map

A, Δ81-SEX4-HIS$_6$ was purified from *E. coli* supernatants using a Profinia IMAC cartridge. The elute was then purified to near homogeneity by separation over a S200 gel filtration column. *B*, A sequence coverage map of pepsin digested peptides identified in the MS/MS experiments. A total of 264 peptides were detected. Solid lines indicate the 28 peptides utilized for our analysis, and dashed lines indicate peptides not used for our analysis. Numbers correspond to full length SEX4 with amino acid 81 beginning with the first threonine in the sequence.

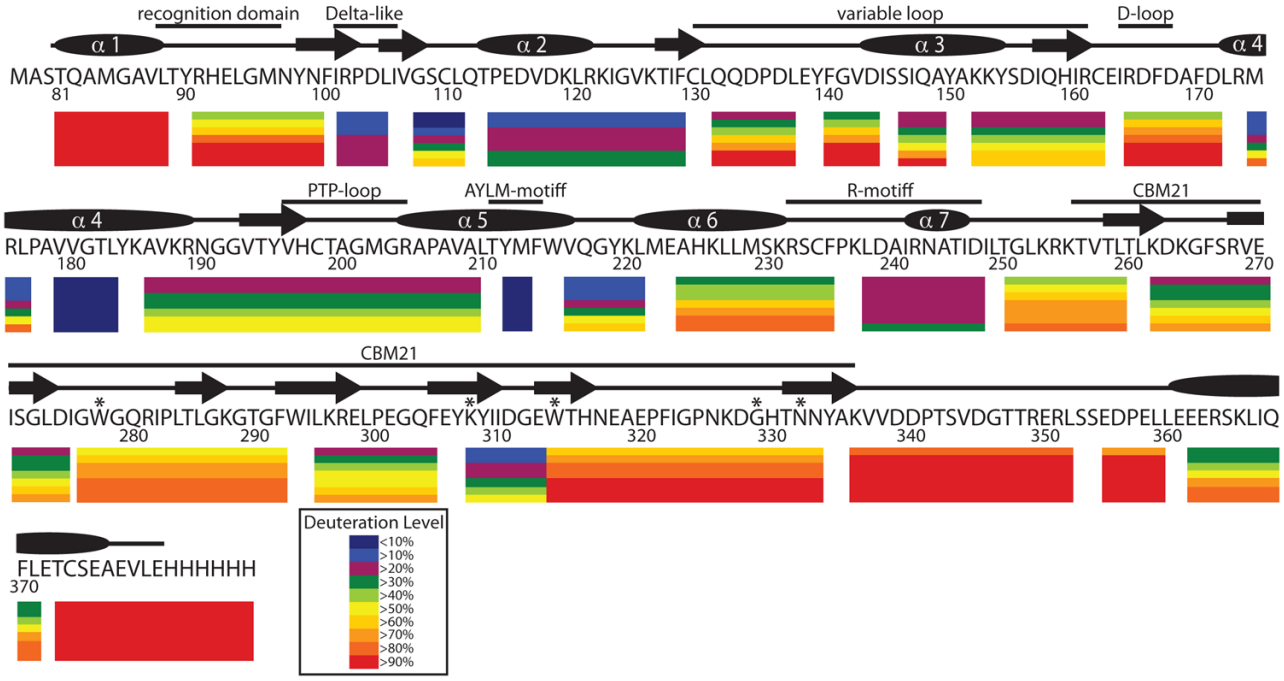

FIGURE 4. H/D exchange results of glucan-free Δ81-SEX4

The deuteration level of glucan-free Δ81-SEX4 (Apo-Δ81-SEX4) shown as lowest deuteration levels in blue to highest deuteration levels in red, as indicated by the inset. Each row represents the peptide we analyzed from Figure 3B. Each bar represents the level of deuteration at one of the seven time points from 10s to 10,000 s (166 min). The DSP domain extends from amino acids 81-249, and important regions are labeled appropriately. The CBM extends from amino acid 256-337. Residues predicted to be necessary for glucan bind are marked with an asterisk. The predicted secondary structure of SEX4 is designated above the amino acids. α-helices in the DSP domain are labeled per standard nomenclature. Amino acid numbers refer to the amino acid positions in full length SEX4. Deuterons from the first two amino acids of each peptide are lacking due to the fact that the first amino acid of each peptide lacks an amide hydrogen and the second amide hydrogen exchanges too rapidly to retain deuterons during processing. Therefore, the exchange data is lacking for the first two amino acids of each peptide in this figure. There is no gap between amino acids 313 and 314 because we analyzed overlapping peptides in this region in order to have exchange data covering W314 since W314 is proposed to play an integral part in glucan binding.

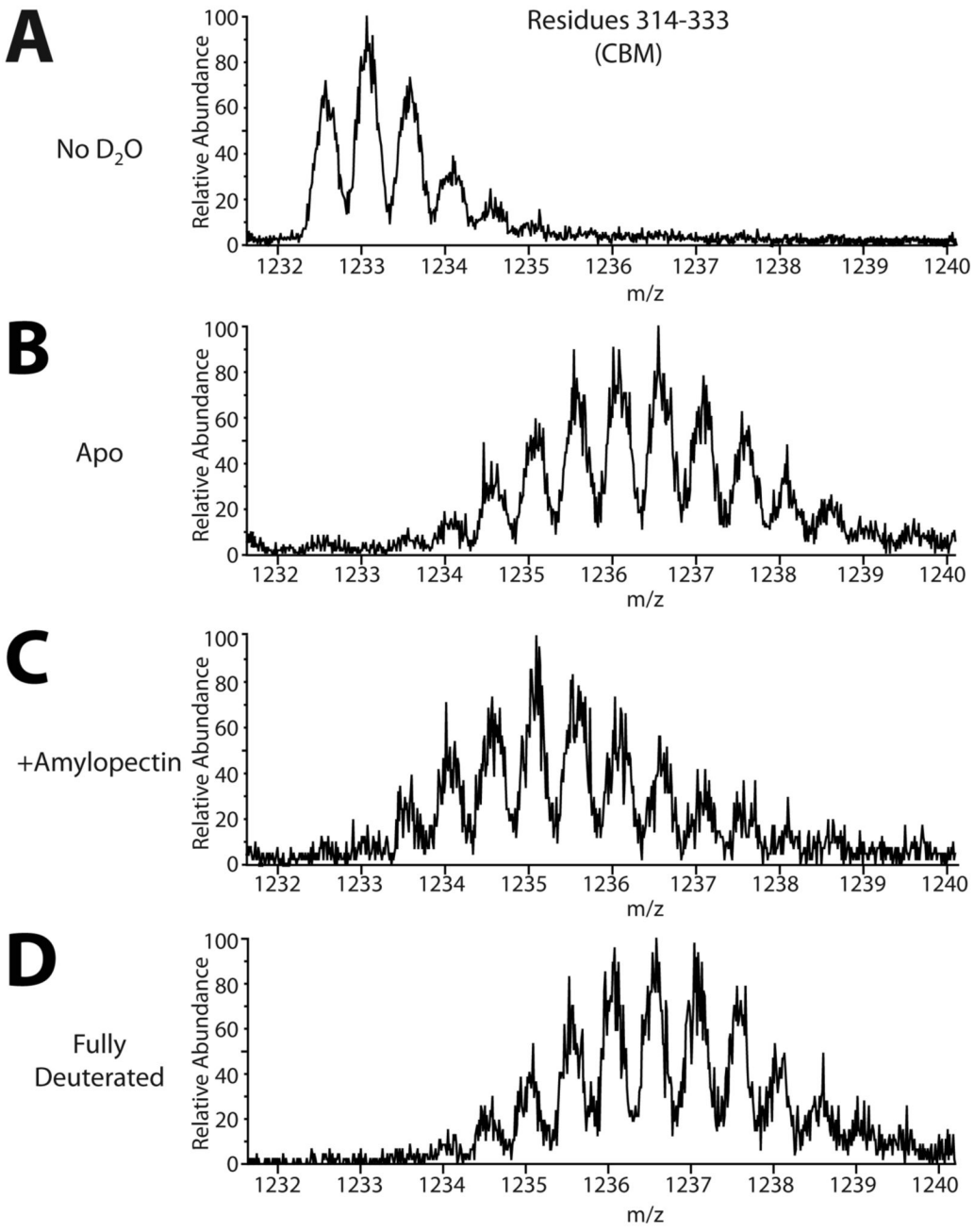

FIGURE 5. Mass spectra of pepsin-treated Δ81-SEX4 residues 312-333

A, The mass spectra of a peptide covering residues 312-333, within the CBM, prior to exposure to D_2O. *B*, The mass spectra of the same peptide as in *A*, but after 3000s exposure to D_2O and in the absence of amylopectin (Apo). Note the increase in complexity and mass compared to *A*. *C*, The mass spectra of the same peptide as in *A* and *B*, but after 3000s exposure to D_2O and in the presence of amylopectin (+Amylopectin). Note the shift to a lower m/z ratio observed with amylopectin binding. *D*, The mass spectra of the same peptide in *A*-*C*, but after being fully deuterated.

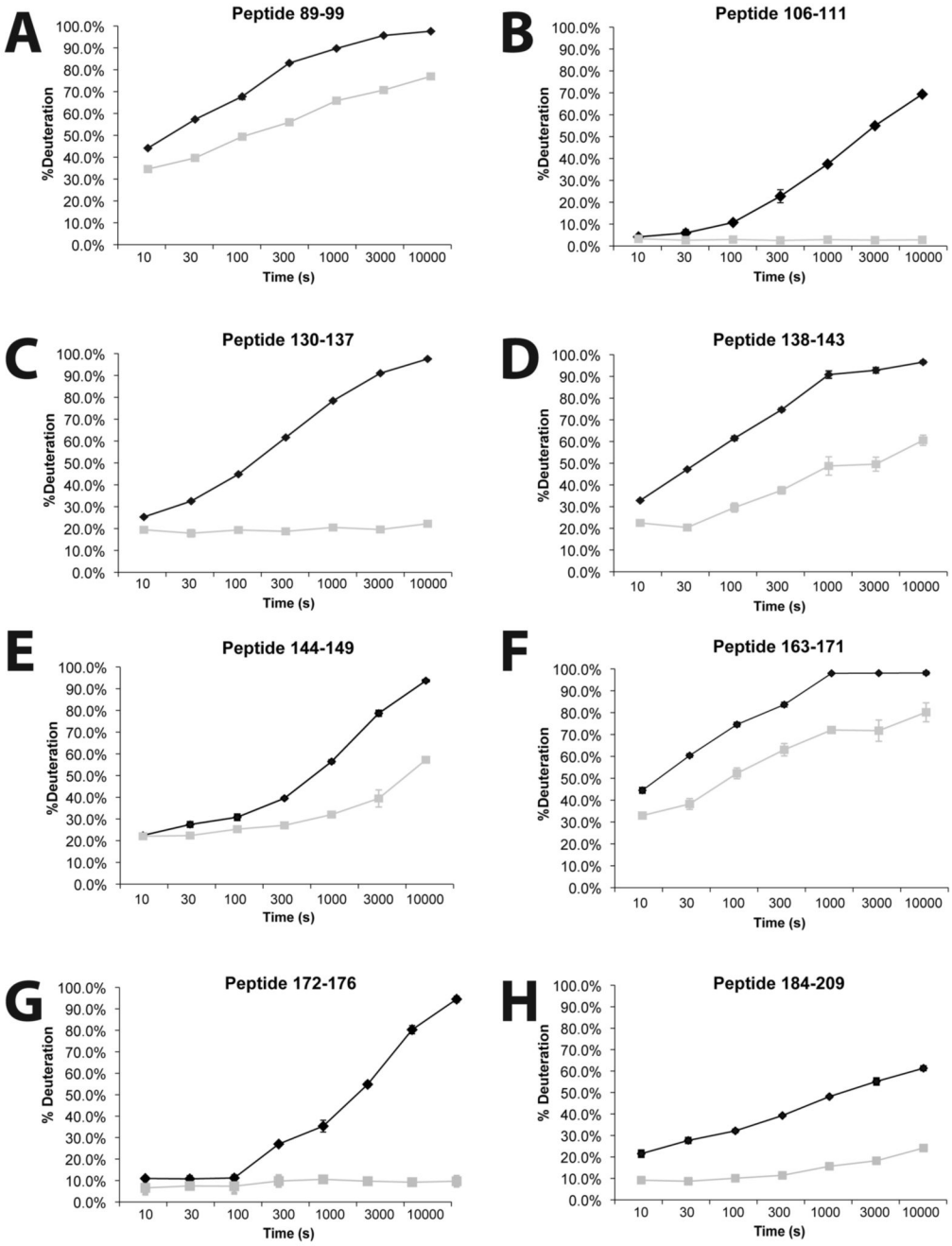

FIGURE 6. DSP domain peptides that exhibited a change in deuterium incorporation for Apo versus amylopectin-bound

Time dependent incorporation in SEX4 peptides *A*, Thr^{89}-Asn^{99}; *B*, Ile^{106}-Leu^{111}; *C*, Cys^{130}-Leu^{137}; *D*, Glu^{138}-Asp^{143}; *E*, Ile^{144}-Ala^{149}; *F*, Glu^{163}-Asp^{171}; *G*, Leu^{172}-Leu^{176}; *H*, Tyr^{184}-Ala^{209}. Data shown in *black diamonds* and *grey squares* represent percentage of deuterium incorporation into Apo- and amylopectin-bound Δ81-SEX4-C/S, respectively, at multiple time points. The x-axis is a log scale.

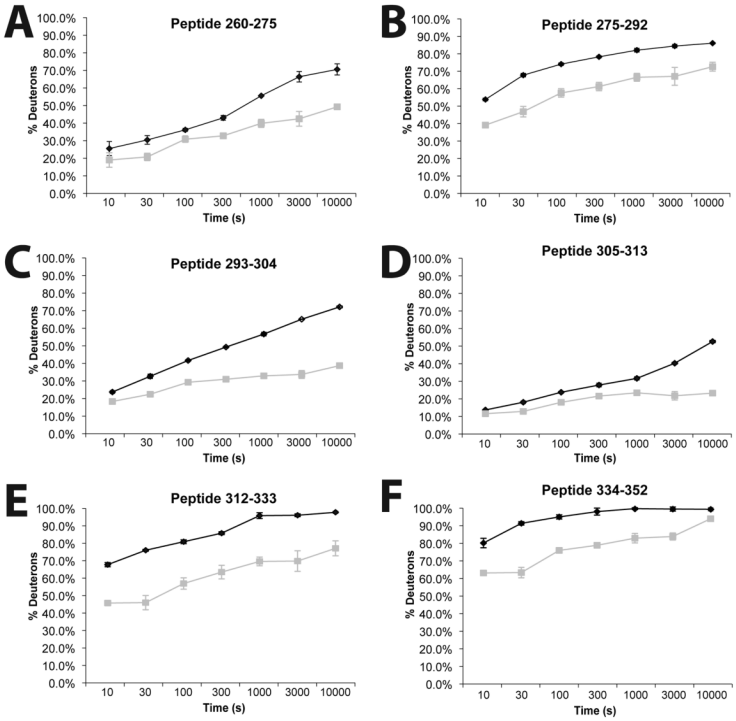

FIGURE 7. CBM peptides that exhibited a change in deuterium incorporation for Apo versus amylopectin-bound

Time dependent incorporation in SEX4 peptides *A*, Thr^{260}-Asp^{275}; *B*, Asp^{275}-Phe^{292}; *C*, Trp^{293}-Phe^{304}; *D*, Glu^{305}-Gly^{313}; *E*, Asp^{312}-Asn^{333}; *F*, Tyr^{334}-Leu^{352}. Data shown in *black diamonds* and *grey squares* represent percentage of deuterium incorporation into Apo- and amylopectin-bound Δ81-SEX4-C/S, respectively, at multiple time points. The x-axis is a log scale.

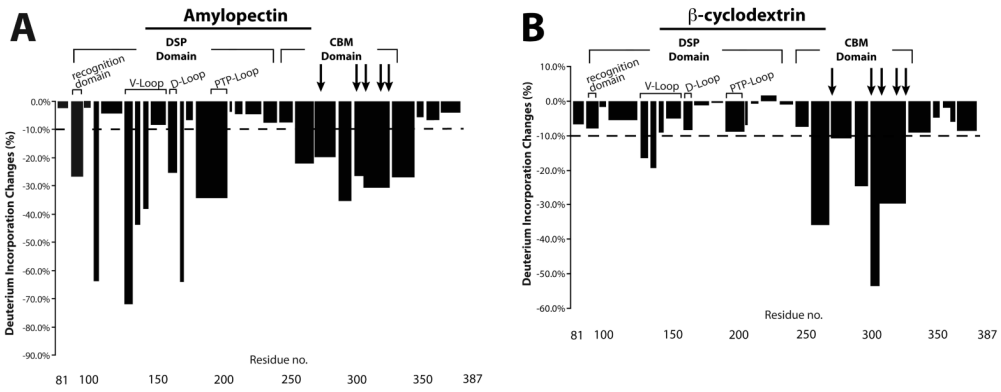

FIGURE 8. Maximal percent decrease in deuteration upon substrate binding

A, A bar graph depicting the maximal percent decrease in deuteration between Apo- Δ81-SEX4 and amylopectin-bound Δ81-SEX4. The different regions of the DSP domain are delineated at the top of the graph and arrows signify the position of residues within the CBM necessary for glucan binding. The residue numbers at the bottom refer to amino acid numbers of full length SEX4. *B*, A similar bar graph as in *A*, with the exception that the comparison is between Apo- Δ81-SEX4 and Δ81-SEX4 in the presence of β-cyclodextrin. In both *A* and *B*, the dotted line designates a less than 10% decrease. Note that the scales are slightly different in *A* and *B*.

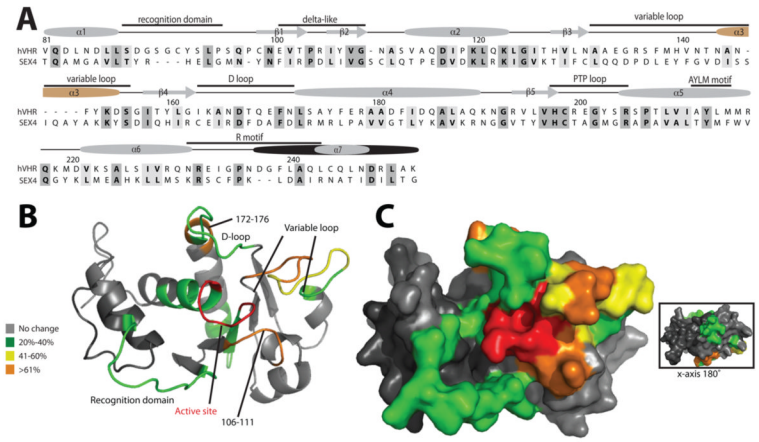

FIGURE 9. DSP domain decreases in percent deuteration upon amylopectin binding

A, An alignment of the DSP domain of human VHR (hVHR) and SEX4. Above the amino acids is a comparison between the predicted secondary structures of the SEX4 DSP domain with the known secondary structure of VHR. The α-helices and β-sheets are numbered per accepted DSP domain nomenclature (59). Grey α-helices and β-sheets represent common structural features between hVHR and SEX4, the tan α-helix 3 represents a structural feature lacking in hVHR but present in SEX4 and in most DSP domains, and the black α-helix 7 represents an extended helix of hVHR compared to the grey predicted helix of SEX4. Numbers above the amino acids refer to their position in full length SEX4. *B*, A ribbon structure of the SEX4 DSP domain model with the percent change in deuteration from Figure 8 mapped onto it. The active site is highlighted in red and percent change corresponds to the inset. The DSP regions of interest are also labeled. *C*, A surface view of the SEX4 DSP domain model with percent change in deuteration mapped onto it. Percent change colors are as in *B*. The inset is a view of the surface after rotating the model 180° on the x-axis. The residues colored green in the center of this view are from peptide 184-209 covering the PTP-loop.

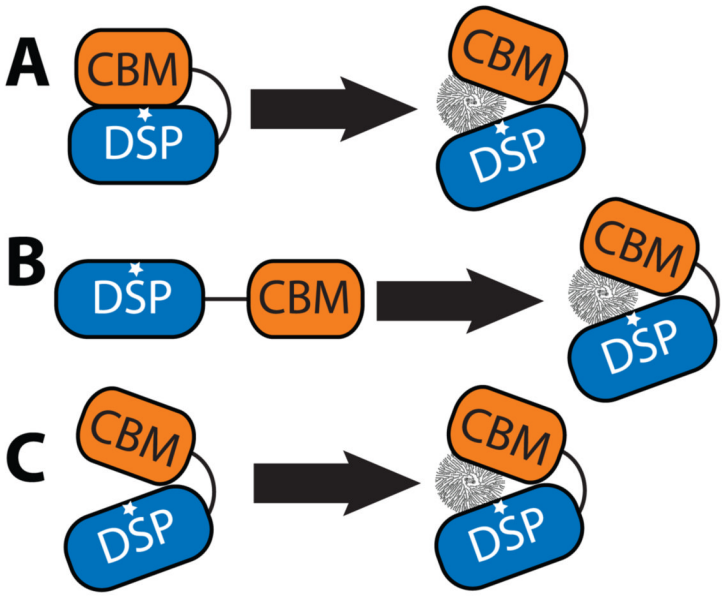

FIGURE 10. Schematic representing possible SEX4 dynamics

A, In this model, the SEX4 CBM binds and precludes substrate entry into the DSP domain active site. Glucan binding triggers a substantial domain rearrangement that allows the active site to become available to the phosphoglucan. *B*, Glucan binding by the CBM generates a global domain rearrangement that brings the glucan into contact with the DSP domain to allow phosphoglucan dephosphorylation. *C*, The CBM binds the phosphoglucan and positions it appropriately so that the DSP comes into contact with the glucan. This binding results in minimal domain rearrangement and presents the phosphoglucan to the DSP domain active site.